Research in Astronomy and Astrophysics, 23:055020 (9pp), 2023 May https://doi.org/10.1088/1674-4527/accb7b

Probing the Internal Physics of Neutron Stars through the Observed Braking Indices and Magnetic Tilt Angles of Several Young Pulsars

Fang-Yuan Hu, Quan Cheng, Xiao-Ping Zheng, Jia-Qian Wang, Yu-Long Yan, Jia-Yu Wang, and Tian-Yu Luo
Institute of Astrophysics, Central China Normal University, Wuhan 430079, China; qcheng@mail.ccnu.edu.cn, zhxp@mail.ccnu.edu.cn
Received 2022 December 21; revised 2023 March 17; accepted 2023 April 3; published 2023 April 28

Abstract

The braking indices of pulsars may contain important information about the internal physics of neutron stars (NSs), such as neutron superfluidity and internal magnetic fields. As a subsequent paper of Cheng et al., we perform the same analysis as that done in the previous paper to other young pulsars with a steady braking index, n. Combining the timing data of these pulsars with the theory of magnetic field decay, and using their measured magnetic tilt angles, we can set constraints on the number of precession cycles, ξ, which represents the interactions between superfluid neutrons and other particles in the NS interior. For the pulsars considered in this paper, the results show that ξ is within the range of a few $\times 10^3$ to a few $\times 10^6$. Interestingly, for the Crab and Vela pulsars, the constraints on ξ obtained with our method are generally consistent with that derived from modeling of the glitch rise behaviors of the two pulsars. Furthermore, we find that the internal magnetic fields of pulsar with $n < 3$ may be dominated by the toroidal components. Our results may not only help to understand the interactions between the superfluid neutrons and other particles in the interior of NSs but also be important for the study of continuous gravitational waves from pulsars.

Key words: stars: neutron – (stars:) pulsars: general – stars: magnetic field – gravitational waves

1. Introduction

Neutron stars (NSs) are extremely compact objects which possess strong magnetic fields, electric fields and gravitational fields. Because of these unique properties, NSs are an excellent laboratory in the universe to test fundamental physics (Watts et al. 2016). NSs that can produce periodic electromagnetic radiation are dubbed as pulsars, and from the observed periodic signals one can obtain the spin periods P of pulsars. Moreover, through precise timing observations, the sudden change of P (glitches), first and even second time derivatives of P of some pulsars can also be measured currently. Using these observational results, some key issues about NS physics can be probed, such as the dense matter equation of state and superfluid physics in NS interiors (Link et al. 1999; Andersson et al. 2012; Ho & Andersson 2012; Ho et al. 2015; Li et al. 2016; Pizzochero et al. 2017; Zhou et al. 2017), interactions (or mutual frictions) between superfluid neutrons and other particles in the interior of NSs (Alpar et al. 1984; Graber et al. 2018; Haskell & Sedrakian 2018; Haskell et al. 2018; Cheng et al. 2019), viscous properties of dense matter (Ho & Andersson 2011; Alford & Schwenzer 2014; Haskell 2015), internal magnetic fields of NSs (Mastrano & Melatos 2012; Cheng et al. 2019), and also physics of NS external magnetosphere (Xu & Qiao 2001; Contopoulos & Spitkovsky 2006; Kou & Tong 2015). In fact, it is widely accepted that the spin-down process of NSs is tightly related to the NS physics and different spin-down mechanisms can lead to different spin-down behaviors of NSs (e.g., Muslimov & Page 1996; Menou et al. 2001; Xu & Qiao 2001; Ho & Andersson 2012; Gourgouliatos & Cumming 2015; Chen & Li 2016; Coelho et al. 2016; De Araujo et al. 2016a; Gao et al. 2017).

The braking index $n = \omega\ddot{\omega}/\dot{\omega}^2$ is a good indicator of the specific spin-down mechanisms of NSs, where $\omega = 2\pi/P$ is the angular velocity of NSs, $\dot{\omega}$ and $\ddot{\omega}$ are the first and the second derivatives of ω, respectively. A brief introduction about the spin-down mechanisms and the resultant braking indices of NSs is summarized in Cheng et al. (2019). Currently, the most convincible conclusion is that the primitive model invoking magnetic dipole (MD) radiation in vacuum (Ostriker & Gunn 1969) is inadequate to account for the observed braking indices of several young pulsars since they all deviate from $n = 3$ (Lyne et al. 2015; Archibald et al. 2016). This may be attributed to the strong magnetic fields of NSs because with the presence of strong external dipole fields, the relativistic particle wind in the magnetosphere can provide an additional braking torque (Xu & Qiao 2001; Kou & Tong 2015), leading to $n < 3$ as observed for the majority of young pulsars with measured braking indices (see Lyne et al. 2015 and references therein). Furthermore, if the dipole fields of NSs decay due to Hall drift and ohmic dissipation, as naturally expected from theoretical perspective (Goldreich & Reisenegger 1992; Aguilera et al. 2008; Gao et al. 2017; Kojima & Suzuki 2020), pulsars possibly have braking indices $n > 3$. Observationally, the braking index of PSR J1640-4631 is measured to be $n = 3.15 \pm 0.03$ (Archibald et al. 2016), which may be the outcome of dipole field decay (Gao et al. 2017). Besides strong external dipole fields, in the interior of NSs even higher internal magnetic fields may also exist (Braithwaite 2009). The NSs will thus deform into a quadrupole ellipsoid and emit gravitational waves (GWs), which represents an alternative scenario in explaining the observed braking index of PSR J1640-4631 (De Araujo et al. 2016b).

In fact, the effect of internal magnetic fields on the braking indices of pulsars is not just reflected in the braking effect of GW radiation. With the presence of strong internal fields, free-body precession of the magnetic axis around spin axis of a deformed NS would occur if the star is not in a state with minimum spin energy (Dall'Osso et al. 2009). The free-body precession of the NS can be damped because of internal viscous dissipation and result in the evolution of the tilt angle between the two axes. Evolution of the NS's magnetic tilt angle also has impact on its observed braking index. Generally, the MD and GW radiation lead to aligned torques between the magnetic and spin axes and thus the tilt angle will decrease with time (Davis & Goldstein 1970; Cutler & Jones 2000; Dall'Osso et al. 2009; Philippov et al. 2014). However, depending on the shape, namely the sign of the ellipticity ϵ_B of magnetic deformation of the NS, damping of free-body precession due to viscosity can either cause the tilt angle to increase (if $\epsilon_B < 0$) or decrease (if $\epsilon_B > 0$) with time (Cutler 2002; Dall'Osso et al. 2009). The sign of ϵ_B is determined by the NS's internal magnetic field configuration. To be specific, if the internal magnetic fields are dominated by the toroidal (poloidal) component, one has $\epsilon_B < 0$ ($\epsilon_B > 0$). Although the results of magnetohydrodynamic simulations show that the internal fields of NSs probably have a twisted-torus shape consist of both the toroidal and the poloidal components (Braithwaite & Spruit 2004, 2006), the dominant part of internal fields in still under debate. This issue is very worthy of investigation since it is crucial for both the study of pulsar timing and that of continuous GWs from pulsars (Dall'Osso et al. 2009; Cheng et al. 2019).

For a magnetically deformed NS, the change rate of the tilt angle due to viscous damping of free-body precession is associated with a critical physical quantity dubbed as the number of precession cycles, ξ (Jones 1976; Alpar et al. 1984; Alpar & Sauls 1988). This quantity represents the specific viscous mechanisms through which the precessional energy of the NS is dissipated during the precession process. In fact, ξ is approximately equal to the reciprocal of the superfluid mutual friction parameter, $\mathcal{B}$ (Cheng et al. 2019), whose exact value is still an open issue (Haskell et al. 2018). Theoretically, if damping of the free-body precession is dominated by the scattering of relativistic electrons off superfluid neutrons in the core of the NS, one has $\xi \approx 10^2$–10^4 (Alpar & Sauls 1988; Dall'Osso et al. 2009; Cheng et al. 2019). On the other hand, if the viscosity essentially comes from the interactions between superfluid neutrons and lattices in the NS crust, the number of precession cycles could be as large as $\xi \approx 10^8$ when phonon excitations govern the interactions, while it could be as small as $\xi \approx 10$ when kelvin mutual friction dominates the interactions (Haskell & Sedrakian 2018; Haskell et al. 2018; Cheng et al. 2019). Modeling of the rising behaviors of some large glitches of the Crab and Vela pulsars showed that the mutual friction parameter is possibly in the range $3 \times 10^{-4} \lesssim \mathcal{B} \lesssim 10^{-5}$ (corresponds to $3.3 \times 10^3 \lesssim \xi \lesssim 10^5$) for the Crab, while $3 \times 10^{-4} \lesssim \mathcal{B} \lesssim 10^{-3}$ (corresponds to $10^3 \lesssim \xi \lesssim 3.3 \times 10^3$) for the Vela (Haskell et al. 2018). Furthermore, from the upper limit on the rise time $\tau_r \leqslant 12.6$ s of the 2016 Vela glitch, Ashton et al. (2019) obtained a lower limit $\mathcal{B} \gtrsim 5.7 \times 10^{-6}$, which corresponds to $\xi \lesssim 1.8 \times 10^5$. Because of the high uncertainty on the value of ξ (and also $\mathcal{B}$), an effective way is needed to constrain its value. In our previous paper (Cheng et al. 2019), we suggested that the observed braking indices of pulsars may help to constrain ξ and provide us clues on the complex interactions between superfluid neutrons and other particles in NSs. It should also be noted that the value of ξ is also crucial in the discussion of continuous GWs from pulsars since it determines the timescales on which the NSs could reach the optimal (adverse) configuration for GW radiation (Dall'Osso et al. 2009; Cheng et al. 2019).

Based on the observed braking index of PSR J1640-4631 and the theory of dipole magnetic field decay, Cheng et al. (2019) showed that constraints on both ξ and the internal magnetic field configuration of this NS may be set if its tilt angle could be measured in future observations. In this paper, following the same method of Cheng et al. (2019), the internal magnetic field configuration of NSs and the value of ξ are constrained by using the observed braking indices and tilt angles of several young pulsars except for PSR B0540-69. We note that for PSR B0540-69, its braking index decreased abruptly from about 2.14 to 0.03 in December 2011 (Livingstone et al. 2007; Marshall et al. 2016). Other mechanisms are needed to interpret its odd evolution behavior (e.g., Ekşi 2017; Horvath 2019), which are beyond the scope of this paper. Here is the framework of our paper. In Section 2, we give a brief introduction about the model used in Cheng et al. (2019). The results are presented in Section 3. Finally, conclusion and discussions are provided in Section 4.

2. Theoretical Model

As generally expected, with the presence of strong internal and external magnetic fields, an isolated NS will spin down via both MD and GW radiation (e.g., Shapiro & Teukolsky 1983). The latter comes from the magnetic deformation of the NS whose quadrupole ellipticity is described by the parameter, ϵ_B. Meanwhile, with the spin-down of the NS, its magnetic tilt angle χ may also evolve with time due to MD and GW radiation, as well as damping of the free-body precession caused by viscous dissipation (Dall'Osso et al. 2009; Cheng et al. 2019). Owing to non-zero resistance in the crust, the dipole field of the NS could decay under the combined effects of Hall drift and ohmic dissipation if it has a crustal origin (e.g., Goldreich & Reisenegger 1992; Aguilera et al. 2008; Kojima & Suzuki 2020). After taking into account all these effects and assuming that a corotating plasma magnetosphere exists outside the NS (Goldreich & Julian 1969; Spitkovsky 2006), the pulsar's braking index can be expressed as (Cheng et al. 2019)

$$n = 3 - \frac{2P}{\dot{P}}\left\{\frac{\dot{B}_{\rm d}}{B_{\rm d}} + \dot{\chi}\sin\chi\cos\chi\left[\frac{1}{1+\sin^2\chi} + \frac{1+30\sin^2\chi}{\eta\sin^2\chi(1+15\sin^2\chi)}\right]\right\}, \tag{1}$$

where $\dot{P}$, $\dot{B}_{\rm d}$, and $\dot{\chi}$ are the first derivatives of spin period P, dipole field $B_{\rm d}$, and tilt angle χ, respectively. $\eta = 5kc^2B_{\rm d}^2R^6(1+\sin^2\chi)/[2G\epsilon_{\rm B}^2I^2\omega^2(1+15\sin^2\chi)\sin^2\chi]$ is the ratio of MD spin-down to GW spin-down rates, where R and I are the radius and moment of inertia of the NS, k the constant related to MD radiation. Following Cheng et al. (2019), we take $R = 10$ km, $I = 10^{45}$ g cm^2, and $k = 1/6$ in this paper. The change rate of the tilt angle $\dot{\chi}$ is determined by MD and GW radiation, and viscous damping of the NS's free-body precession. The specific form of $\dot{\chi}$ is given by Cheng et al. (2019):

$$\dot{\chi} = \begin{cases} -\dfrac{kB_{\rm d}^2R^6\omega^2}{Ic^3}\sin\chi\cos\chi \\ -\dfrac{2G}{5c^5}I\epsilon_{\rm B}^2\omega^4\sin\chi\cos\chi(15\sin^2\chi+1) - \dfrac{\epsilon_{\rm B}}{\xi P}\tan\chi, & \text{for } \epsilon_{\rm B} > 0 \\ -\dfrac{kB_{\rm d}^2R^6\omega^2}{Ic^3}\sin\chi\cos\chi - \dfrac{2G}{5c^5}I\epsilon_{\rm B}^2\omega^4\sin\chi\cos\chi(15\sin^2\chi+1) \\ -\dfrac{\epsilon_{\rm B}}{\xi P}\cot\chi, & \text{for } \epsilon_{\rm B} < 0. \end{cases} \tag{2}$$

In the above equation, the first and second terms represent the decrease of χ caused by MD and GW radiation, respectively. The third term depicts the evolution of χ due to viscous damping of the stellar free-body precession, whose form actually depends on the sign of $\epsilon_{\rm B}$, as mentioned in the previous section.

The ellipticity $\epsilon_{\rm B}$ is dependent on the internal magnetic energy, the NS's internal magnetic field configuration, and the NS EOS (Haskell et al. 2008; Dall'Osso et al. 2009). The specific forms of $\epsilon_{\rm B}$ used in this paper are given in Cheng et al. (2019). We emphasize that the two forms of $\epsilon_{\rm B}$ used in Cheng et al. (2019) represent two different internal magnetic field configurations, namely the poloidal-dominated ($\epsilon_{\rm B} > 0$) versus toroidal-dominated ($\epsilon_{\rm B} < 0$) configurations. The two different configurations naturally lead to different tilt angle evolution behaviors, as shown in Equation (2) above.

The dipole field decay rate $\dot{B}_{\rm d}$ in Equation (1) can be derived from the theory of magnetic field decay. It is possible that decay of the dipole field follows a simple exponential form $\dot{B}_{\rm d} = -B_{\rm d}/\tau_{\rm D}$ with $\tau_{\rm D}$ representing the field decay timescale (Pons et al. 2007; Dall'Osso et al. 2012; Cheng et al. 2019). The specific form of $\tau_{\rm D}$ is still uncertain. Theoretical calculations showed that if Hall drift dominates the field decay process by changing the large scale field into small ones, the field decay timescale could be determined by the Hall timescale, that is, $\tau_{\rm D} = \tau_{\rm H} \simeq 1.2\times10^4(B_{\rm d}/10^{15}\,{\rm G})^{-1}$ yr (Cumming et al. 2004; Dall'Osso et al. 2012). As $B_{\rm d}$ can be substituted by χ via $B_{\rm d} = \left[-\frac{\dot{\omega}Ic^3}{k\omega^3R^6(1+\sin^2\chi)}\right]^{1/2}$ (Cheng et al. 2019), the Hall timescale can be expressed as a function of χ, as shown by the black solid line in the left panel of Figure 1. On the other hand, if ohmic dissipation plays an important role in decay of the crustal fields of NSs, we may have a constant decay timescale (irrelevant to $B_{\rm d}$) with possible values $\tau_{\rm D} = \tau_{\rm O} = 5\times10^5$, 10^6, or even 1.5×10^8 yr (Pons et al. 2007; Bransgrove et al. 2018; Cheng et al. 2019). These ohmic timescales are represented by the black dashed, dotted, and dashed–dotted (also the upper boundary of the blank region) lines in the left panel of Figure 1, respectively. For detailed discussions about these timescales, one can refer to Cheng et al. (2019). Finally, if the dipole field decays because of the combined effects of Hall drift and ohmic dissipation, the field decay timescale possibly has the form $\tau_{\rm D} = 1/[1/\tau_{\rm H} + 1/\tau_{\rm O}]$. In this case, by adopting $\tau_{\rm O} = 5\times10^5$ yr, we can obtain the $\tau_{\rm D}$–χ curve, which is shown by the black dashed–dotted-dotted line (also the lower boundary of the blank region) in the left panel of Figure 1.

After substituting Equation (2) into Equation (1) and using the observed P, $\dot{P}$, and n of a pulsar, by solving Equation (1) we can obtain the evolution curve of $\tau_{\rm D}(=-B_{\rm d}/\dot{B}_{\rm d})$ versus χ for a specific ξ, as that done in Cheng et al. (2019) for PSR J1640-4631. Obviously, here the $\tau_{\rm D}$–χ curve is obtained from the pulsar's timing data. If the tilt angle of the pulsar can be measured, we can then set constraints on ξ. The method of determining the value of ξ for a specific χ measured was illustrated in Cheng et al. (2019). By taking PSR J1734-3333 as an example, a brief introduction about this method will be given in the next section. In Table 1, we list the observed P, $\dot{P}$, n, and χ of several young pulsars with a steady braking index. These data is partially taken from De Araujo et al. (2016c) and references therein. Obviously, all these pulsars have braking indices $n < 3$. For these pulsars, we investigate what their timing data can tell us about the value of ξ and their internal magnetic field configurations. Same as in Cheng et al. (2019), the error bars in values of n are neglected in the calculations.

3. Results

We first investigate how the timing data and measured tilt angles of these pulsars can help to constrain the value of ξ. We stress that for pulsars with $n < 3$, the constraints on ξ are

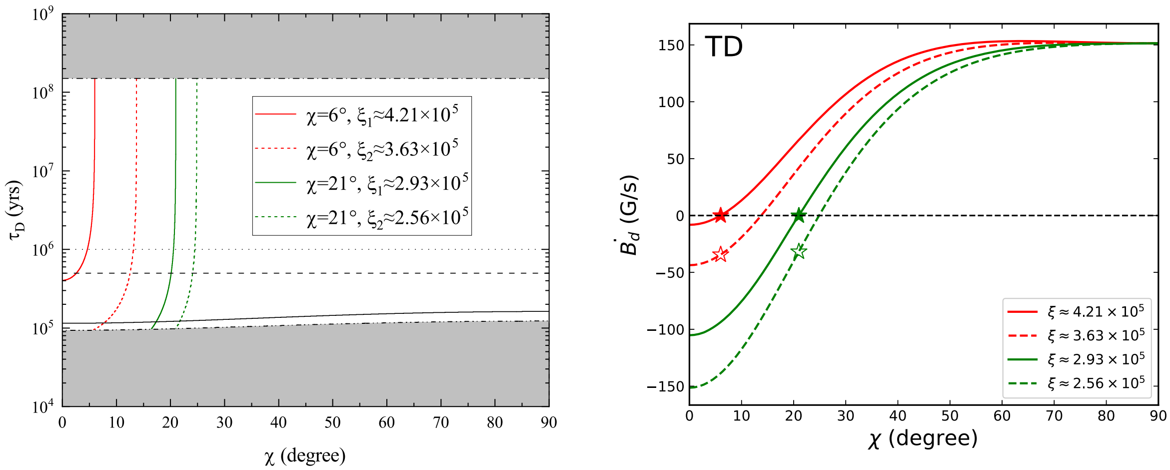

Figure 1. (Left) Evolution of the dipole field decay timescale $\tau_{\rm D}$ with the tilt angle χ for PSR J1734-3333. The black curves are obtained based on the theory of magnetic field decay. The colored curves are derived by using the timing data of this pulsar and possible values of the tilt angle observed, and assuming that the internal magnetic fields of this pulsar are toroidal-dominated (TD). The colored solid and dashed lines respectively determine the upper and lower limits of ξ at a specific χ, as shown in the legends. (Right) Evolution of the dipole field decay rate $\dot{B}_{\rm d}$ vs. the tilt angle χ for PSR J1734-3333. The result is for the case of TD internal fields. The $\dot{B}_{\rm d}-\chi$ curves are calculated for different values of ξ adopted, as shown in the legends. The values of $\dot{B}_{\rm d}$ that correspond to the upper and lower limits of ξ derived at $\chi=6°$ and 21° are respectively shown by the stars with different types and colors. The black dashed line corresponds to $\dot{B}_{\rm d}=0$. See the text for details of the two panels in this figure.

Table 1
The Measured Period P, its First Derivative $\dot{P}$, Braking Index n, and Measured Magnetic Tilt Angles χ of Several Young Pulsars with a Steady Braking Index

Pulsar Name	P (s)	$\dot{P}$ (10^{-13} s/s)	n	χ	References
PSR J1734-3333	1.17	22.8	0.9 ± 0.2	6°, 21°	(1), (2)
PSR B0833-45 (Vela)	0.089	1.25	1.4 ± 0.2	62°, 70°, 75°, 79°	(3), (4), (5), (6)
PSR J1833-1034	0.062	2.02	1.8569 ± 0.0006	70°	(7), (8)
PSR J1846-0258	0.324	71	2.19 ± 0.03	10°	(9), (10)
PSR B0531 + 21 (Crab)	0.033	4.21	2.51 ± 0.01	45°, 60°, 70°	(4), (5), (11), (12), (13)
PSR J1119-6127	0.408	40.2	2.684 ± 0.002	7°, 16°, 21°	(14), (15), (16), (17)
PSR J1513-5908	0.151	15.3	2.839 ± 0.001	3°, 10°	(2), (18)

References. (1) Espinoza et al. (2011), (2) Nikitina & Malov (2017), (3) Lyne et al. (1996), (4) Watters et al. (2009), (5) Dyks & Rudak (2003), (6) Barnard et al. (2016), (7) Roy et al. (2012), (8) Li et al. (2013), (9) Archibald et al. (2015), (10) Wang et al. (2014), (11) Lyne et al. (1993), (12) Harding et al. (2008), (13) Du et al. (2012), (14) Weltevrede et al. (2011), (15) Rookyard et al. (2015a), (16) Rookyard et al. (2015b), (17) Tian (2018), (18) Livingstone et al. (2007).

obtained based on the assumption that their internal magnetic fields are toroidal-dominated. The reason is that in order to account for the timing data of these pulsars, the assumption of poloidal-dominated internal fields will be in conflict with the field-decay requirement, as we will show later in this section. The result for PSR J1734-3333 is presented in the left panel of Figure 1. The possible values of the tilt angle of PSR J1734-3333 are measured to be $\chi=6°$ and 21° (Nikitina & Malov 2017). As stated above, by using the timing data of a pulsar and solving Equation (1), the $\tau_{\rm D}$–χ curve can be obtained. Furthermore, by changing the value of ξ to ensure that the $\tau_{\rm D}$–χ curve obtained from the timing data of PSR J1734-3333 intersects with the $\tau_{\rm D}$–χ curve obtained from the theory of magnetic field decay at one of the measured values $\chi=6°$, we can obtain the value of ξ. Since in our model, the $\tau_{\rm D}$–χ curve obtained from the theory of magnetic field decay can be any of the five black lines in the left panel of Figure 1, hence by changing the value of ξ five intersections can be found for $\chi=6°$. We can thus approximately obtain the range of ξ, whose upper limit is derived by requiring that the $\tau_{\rm D}$–χ obtained from the timing data of PSR J1734-3333 intersects with the upper boundary of the blank region at $\chi=6°$. As presented in the left panel of Figure 1, the corresponding value of the upper limit is $\xi \approx 4.21 \times 10^5$. The $\tau_{\rm D}$–χ curve obtained from the timing data of PSR J1734-3333 for $\xi \approx 4.21 \times 10^5$ is shown by the red solid line in the left panel of Figure 1. The lower limit, on the other hand, is obtained by requiring that the $\tau_{\rm D}$–χ curve derived based on the timing data intersects with the lower boundary of the blank region at $\chi=6°$. The lower limit can thus be derived as $\xi \approx 3.63 \times 10^5$. As shown in the left

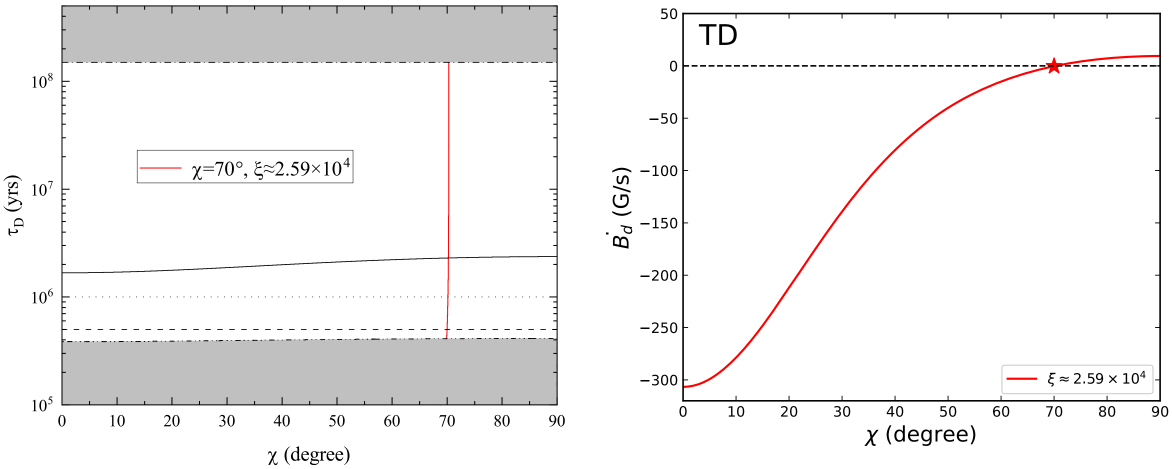

Figure 2. The same as Figure 1, the result for PSR J1833-1034 is shown. For this pulsar, ξ is approximately constrained to be a specific value of 2.59×10^4 due to its large χ measured. Consequently, the value of $\dot{B}_{\rm d}$ at $\chi = 70°$ is also constrained to be a specific value (see the red solid star in the right panel), which is actually negative.

panel of Figure 1, for $\xi \approx 3.63 \times 10^5$, the $\tau_{\rm D}$–χ curve derived based on the timing data is presented by the red dashed line. Therefore, for $\chi = 6°$, the number of precession cycles is constrained to be within the range $3.63 \times 10^5 \lesssim \xi \lesssim 4.21 \times 10^5$. Obviously, with the decrease of ξ, the $\tau_{\rm D}$–χ curve derived based on the timing data gradually shifts toward the direction of larger χ. Similarly, to ensure that the intersections are located at $\chi = 21°$, we have the range $2.56 \times 10^5 \lesssim \xi \lesssim 2.93 \times 10^5$. The $\tau_{\rm D}$–χ curves derived based on the timing data of PSR J1734-3333 for $\xi \approx 2.93 \times 10^5$ and 2.56×10^5 are respectively shown by the green solid and dashed lines in the left panel of Figure 1. Again, it is proved that the measurement of χ of a pulsar could help to constrain the value of ξ, as suggested in Cheng et al. (2019). Here we further suggest that if χ of a pulsar can be precisely measured in future observations, more stringent constraints may be set on ξ, as one can see from the result of PSR J1734-3333.

The same analysis is also performed for other pulsars focused in this paper. The results are respectively shown in the left panels of Figures 2–7. It should be noted that for pulsars whose tilt angles are relatively large, such as PSR J1833-1034, the Crab, and the Vela, we can approximately obtain a specific value (not a range) for ξ at any χ measured. As we know from the left panel of Figure 1, the upper and lower limits of ξ are obtained by requiring that the $\tau_{\rm D} - \chi$ curve derived from the timing data intersects with the upper and lower boundaries of the blank region at an observed χ, respectively. Therefore, for a relatively large χ, the difference between the upper and lower limits of ξ is very tiny. The tilt angle of PSR J1833-1034 is observed to be $\chi = 70°$ (Roy et al. 2012; Li et al. 2013), we thus have $\xi \approx 2.59 \times 10^4$, as presented in the left panel of Figure 2. For PSR J1846-0258, it has a small tilt angle of $\chi = 10°$, we thus have $2.88 \times 10^5 \lesssim \xi \lesssim 2.93 \times 10^5$ (see the left panel of Figure 3). Since χ of PSR J1119-6127 has three possible values (Rookyard et al. 2015a, 2015b; Tian 2018), the corresponding ranges for ξ are $9.84 \times 10^5 \lesssim \xi \lesssim 1.14 \times 10^6$, $6.87 \times 10^5 \lesssim \xi \lesssim 7.73 \times 10^5$, and $5.44 \times 10^5 \lesssim \xi \lesssim 6.03 \times 10^5$, as shown in the left panel of Figure 4. For PSR J1513-5908, its observed χ result in two ranges of $2.05 \times 10^6 \lesssim \xi \lesssim 2.40 \times 10^6$ and $1.53 \times 10^6 \lesssim \xi \lesssim 1.73 \times 10^6$ (see the left panel of Figure 5).

Particular attention is paid to the results of the Crab and Vela pulsars since a comparison of the constraints on ξ obtained in this paper and that derived from glitch observations (Haskell et al. 2018; Ashton et al. 2019) can be made. The tilt angle of the Crab pulsar was observed to have three possible values $\chi = 45°$, $60°$, and $70°$ (Dyks & Rudak 2003; Harding et al. 2008; Watters et al. 2009; Du et al. 2012). From the left panel of Figure 6, one can see that these values respectively correspond to $\xi \approx 1.35 \times 10^5$, 6.25×10^4, and 2.96×10^4. As mentioned in Section 1, by modeling the rising behaviors of three large glitches of the Crab pulsar, the mutual friction parameter $\mathcal{B}$ can be constrained (Haskell et al. 2018). From their results, the number of precession cycles is inferred to be within the range $3.3 \times 10^3 \lesssim \xi \lesssim 10^5$ for the Crab. Therefore, for the Crab pulsar, our constraints on ξ are generally consistent with that obtained in Haskell et al. (2018). On the other hand, for the Vela pulsar, observations showed that its tilt angle may have the following values $\chi = 62°$, $70°$, $75°$, and $79°$ (Dyks & Rudak 2003; Watters et al. 2009; Barnard et al. 2016), which respectively correspond to $\xi \approx 5.51 \times 10^4$, 2.76×10^4, 1.56×10^4, and 8.35×10^3 (see the left panel of Figure 7). Thus for the Vela pulsar, one can see that by using our method, ξ is constrained to have larger values as compared to the results inferred from Haskell et al. (2018). However, our constraints on ξ are consistent with that inferred from Ashton et al. (2019),

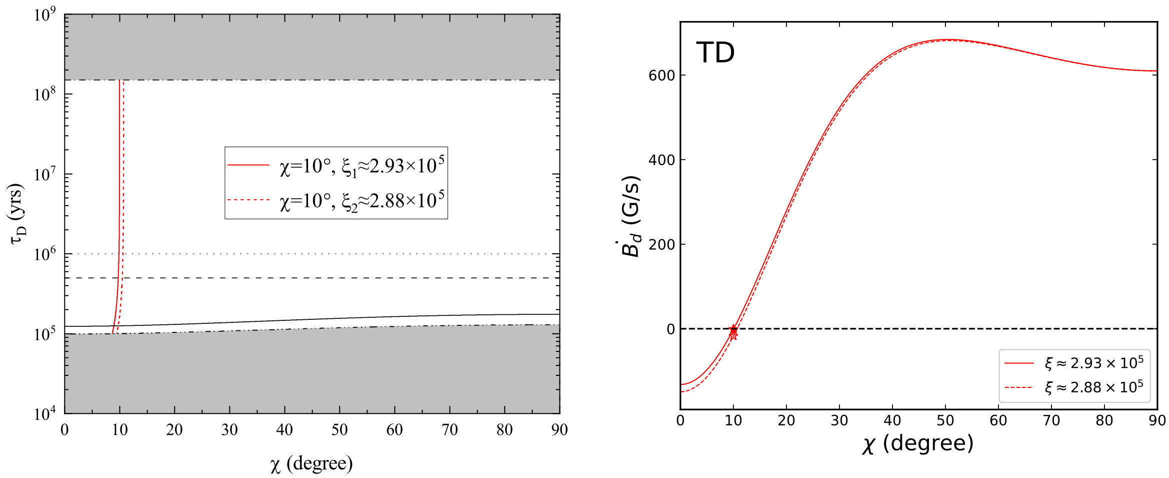

Figure 3. The same as Figure 1, the result for PSR J1846-0258 is shown.

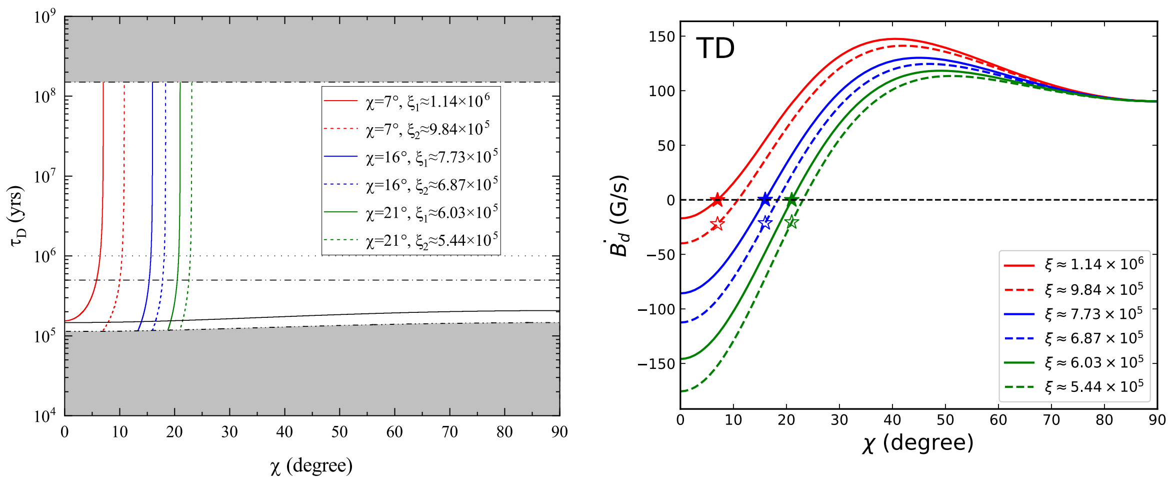

Figure 4. The same as Figure 1, the result for PSR J1119-6127 is shown.

in which a more stringent constraint on the rise time of 2016 Vela glitch was used to constrain the value of $\mathcal{B}$.

We now focus on what constraints on the internal magnetic field configurations can be set from the measured timing data and tilt angles of these pulsars. As the dipole fields of pulsars are required to decay with time ($\dot{B}_{\rm d} < 0$) in this paper, hence not all internal magnetic configurations can satisfy the observed timing data of pulsars above. Obviously, if the internal fields of the pulsars are poloidal-dominated ($\epsilon_{\rm B} > 0$), from Equation (2) we have $\dot{\chi} < 0$. By substituting P, $\dot{P}$, n, and Equation (2) (for $\epsilon_{\rm B} > 0$) into Equation (1), in order to account for the observed braking indices of $n < 3$, one always has $\dot{B}_{\rm d} > 0$ regardless of the value of ξ, inconsistent with the field-decay requirement. On the other hand, if the internal fields of a pulsar are toroidal-dominated, after substituting P, $\dot{P}$, n, and Equation (2) (for $\epsilon_{\rm B} < 0$) into Equation (1), and taking a value that derived above for ξ, we can obtain the $\dot{B}_{\rm d} - \chi$ curve. Then from this evolution curve we can determine the sign of $\dot{B}_{\rm d}$ at a specific χ measured. If the sign is found to be negative, then it is consistent with the field-decay requirement, hence we can conclude that the internal fields of this pulsar are probably toroidal-dominated. To be specific, the result for PSR J1734-3333 is shown in the right panel of Figure 1, which presents the evolution of $\dot{B}_{\rm d}$ versus χ for different values of ξ adopted. As shown in the legends, the values of ξ are respectively its upper and lower limits derived at $\chi = 6°$ and $21°$. The red solid and hollow stars respectively represent $\dot{B}_{\rm d}$ calculated at $\chi = 6°$ for $\xi \approx 4.21 \times 10^5$ and 3.63×10^5, while the green solid and hollow stars show $\dot{B}_{\rm d}$

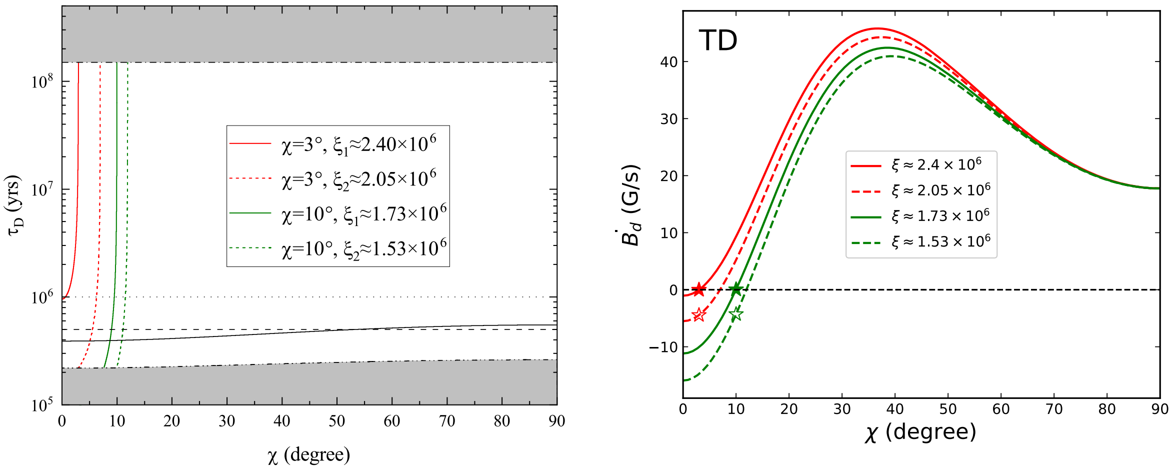

Figure 5. The same as Figure 1, the result for PSR J1513-5908 is shown.

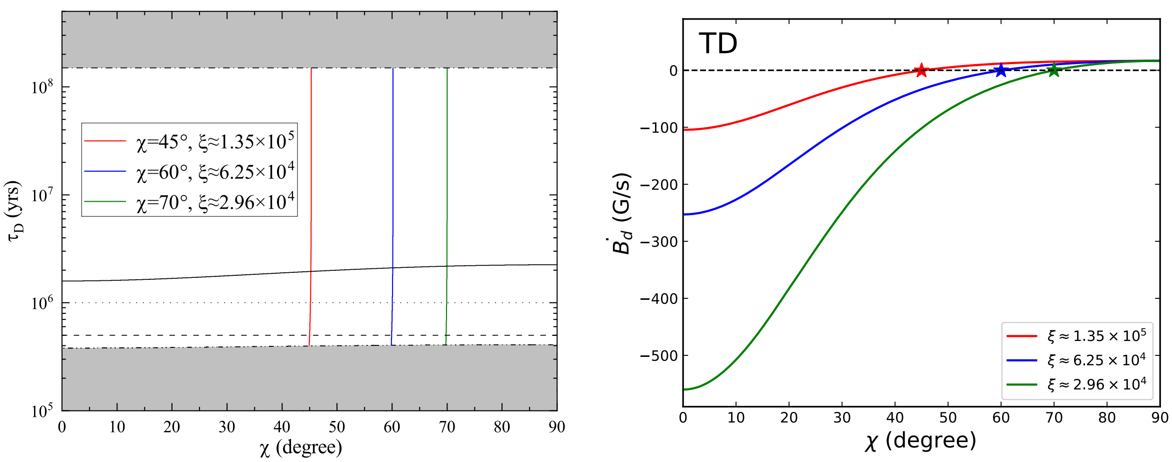

Figure 6. The same as Figure 1, the result for the Crab pulsar is shown. Similar to PSR J1833-1034, because the measured values of χ of this pulsar are large, specific values for ξ can be approximately derived (see the left panel). The colored solid stars in the right panel show $\dot{B}_{\rm d}$ at possible values of χ observed, and at these points we actually have $\dot{B}_{\rm d} < 0$.

derived at $\chi = 21°$ for $\xi \approx 2.93 \times 10^5$ and 2.56×10^5, respectively. From the right panel of Figure 1 we can see that if the internal fields of PSR J1734-3333 are toroidal-dominated, by using the upper and lower limits of ξ obtained at $\chi = 6°$ and $21°$, the dipole field decay rates calculated by solving Equation (1) all satisfy $\dot{B}_{\rm d} < 0$,[1] which are consistent with the field-decay requirement. The same analysis is also performed for other pulsars, the results are respectively shown in the right panels of Figures 2–7. It is found that if the internal fields of these pulsars are dominated by the toroidal part, from Equation (1) the resultant dipole field decay rates at specific χ observed all satisfy $\dot{B}_{\rm d} < 0$. Therefore, for young pulsars with $n < 3$, their internal fields are probably toroidal-dominated.

4. Conclusion and Discussions

As a subsequent paper of Cheng et al. (2019), we perform the same analysis as that done in the previous paper to other young pulsars with a steady braking index. Again, it is proved that by using the timing data of a pulsar and the theory of magnetic field decay, constraints on ξ can be set if χ of this pulsar can be measured. For the seven young pulsars considered in this paper, depending on the measured χ of these pulsars, ξ is constrained to be within the range of a few$\times 10^3$ to a few$\times 10^6$. Most interestingly, for the Crab and Vela pulsars, our constraints on ξ are generally consistent with the results obtained from glitch rise time observations. In view

[1] It should be noted that though the red and green solid stars in the right panel of Figure 1 are quite close to the line of $\dot{B}_{\rm d} = 0$, the values of $\dot{B}_{\rm d}$ at the two points are actually negative.

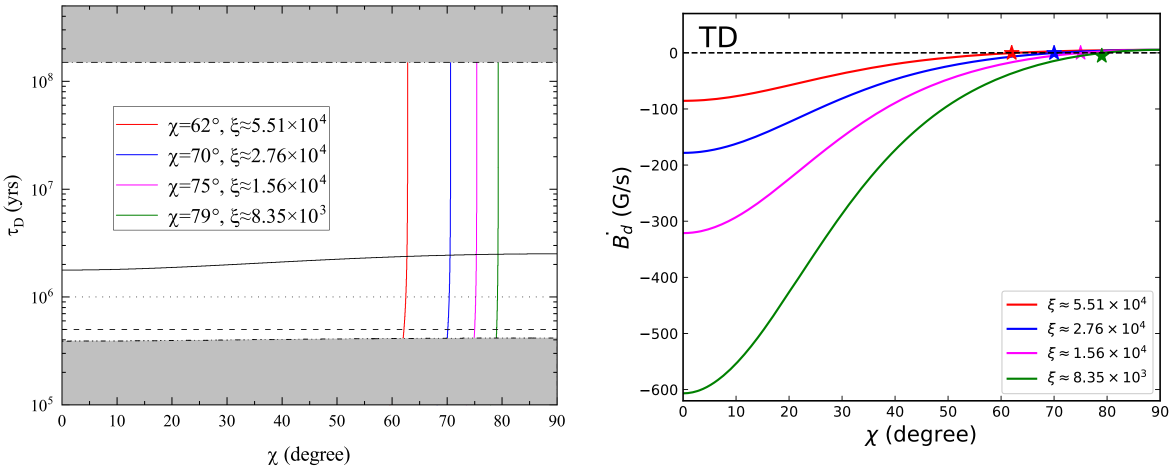

Figure 7. The same as Figure 6, the result for the Vela pulsar is shown.

of the consistency, our method is possibly an effective way to constrain ξ. Furthermore, we find that the internal magnetic fields of NSs with $n < 3$ may be dominated by the toroidal components. Therefore, our method is also potentially an effective way of probing the internal field configuration of NSs.

Our results may be important for the understanding of complicated interactions between superfluid neutrons and other particles in NS interiors. From the ranges of ξ derived for the Crab and Vela pulsars, we suggest that in their interiors the interaction between superfluid neutrons and relativistic electrons may play a dominant role in viscous damping of free-body precession of the NSs. For the majority of young pulsars with larger ξ obtained in this work, relatively weak interactions between superfluid neutrons and crystal lattices may be responsible for the dissipation of the precessional energy of these NSs (Haskell et al. 2018). Moreover, the constraints on ξ may also contribute to the study of continuous GWs from pulsars. As generally expected, the tilt angle of a NS may be initially very tiny. If the NS has toroidal-dominated internal magnetic fields as inferred in this work from some young pulsars, the timescale on which it could reach the optimal configuration ($\chi = \pi/2$) for GW radiation is $\tau_{\rm o} \simeq \xi P/|\epsilon_{\rm B}|$ (Cutler 2002; Stella et al. 2005). Therefore, a large ξ with value $\sim 10^5$–10^6 as obtained for the majority of young pulsars investigated here, may indicate a long timescale for reaching the optimal configuration. Before the optimal configuration is reached, a large amount of spin energy of the NS could be lost via MD rather than GW radiation, leading to weak GW radiation from the NS.

Some intriguing issues still remain to be resolved in future work. The first one is why our method and that by modeling the glitch rise behaviors of the Crab and Vela pulsars (Haskell et al. 2018; Ashton et al. 2019) can result in generally consistent constraints on ξ. Further quantitative analysis is needed to reveal the essence of this consistency. It is also important to test the consistency by using observations of other pulsars provided that their delayed spin-up behaviors, braking indices, and tilt angles can be measured. Second, a quantitative study on the continuous GW radiation from pulsars is also necessary, especially when considering that quite a few pulsars may have toroidal-dominated internal magnetic fields. Moreover, when calculating the GW radiation from pulsars, it is also meaningful to take into account the constraints on ξ derived in this paper. Finally, in order to test the robustness of our results, other forms of magnetic field decay should also be considered in principle. Our future work will be focused on the issues raised above.

Acknowledgments

We gratefully thank the anonymous referee for helpful comments. This work is supported by the National Natural Science Foundation of China (Grant Nos. 12003009, and 12033001), CAS “Light of West China” Program (Grant No. 2019-XBQNXZ-B-016), and the National SKA program of China (Grant No. 2020SKA0120300).

References

Aguilera, D. N., Pons, J. A., & Miralles, J. A. 2008, A&A, 486, 255
Alford, M. G., & Schwenzer, K. 2014, PhRvL, 113, 251102
Alpar, A., & Sauls, J. A. 1988, ApJ, 327, 723
Alpar, M. A., Langer, S. A., & Sauls, J. A. 1984, ApJ, 282, 533
Andersson, N., Glampedakis, K., Ho, W. C. G., & Espinoza, C. M. 2012, PhRvL, 109, 241103
Archibald, R. F., Kaspi, V. M., Beardmore, A. P., Gehrels, N., & Kennea, J. A. 2015, ApJ, 810, 67
Archibald, R. F., Gotthelf, E. V., Ferdman, R. D., et al. 2016, ApJL, 819, L16
Ashton, G., Lasky, P. D., Graber, V., & Palfreyman, J. 2019, NatAs, 3, 1143
Barnard, M., Venter, C., & Harding, A. K. 2016, ApJ, 832, 107
Braithwaite, J. 2009, MNRAS, 397, 763
Braithwaite, J., & Spruit, H. C. 2004, Natur, 431, 819
Braithwaite, J., & Spruit, H. C. 2006, A&A, 450, 1097

Bransgrove, A., Levin, Y., & Beloborodov, A. 2018, MNRAS, 473, 2771
Chen, W. C., & Li, X. D. 2016, MNRAS, 455, L87
Cheng, Q., Zhang, S. N., Zheng, X. P., & Fan, X. L. 2019, PhRvD, 99, 083011
Coelho, J. G., Pereira, J. P., & de Araujo, J. C. N. 2016, ApJ, 823, 97
Contopoulos, I., & Spitkovsky, A. 2006, ApJ, 643, 1139
Cumming, A., Arras, P., & Zweibel, E. 2004, ApJ, 609, 999
Cutler, C. 2002, PhRvD, 66, 084025
Cutler, C., & Jones, D. I. 2000, PhRvD, 63, 024002
Dall'Osso, S., Granot, J., & Piran, T. 2012, MNRAS, 422, 2878
Dall'Osso, S., Shore, S. N., & Stella, L. 2009, MNRAS, 398, 1869
Davis, L., & Goldstein, M. 1970, ApJL, 159, L81
De Araujo, J. C. N., Coelho, J. G., & Costa, C. A. 2016a, ApJ, 831, 35
De Araujo, J. C. N., Coelho, J. G., & Costa, C. A. 2016b, JCAP, 07, 023
De Araujo, J. C. N., Coelho, J. G., & Costa, C. A. 2016c, EPJC, 76, 481
Du, Y. J., Qiao, G. J., & Wang, W. 2012, ApJ, 748, 84
Dyks, J., & Rudak, B. 2003, ApJ, 598, 1201
Ekşi, K. Y. 2017, MNRAS, 469, 1974
Espinoza, C. M., Lyne, A. G., Kramer, M., Manchester, R. N., & Kaspi, V. M. 2011, ApJL, 741, L13
Gao, Z. F., Wang, N., Shan, H., Li, X. D., & Wang, W. 2017, ApJ, 849, 19
Goldreich, P., & Julian, W. H. 1969, ApJ, 157, 869
Goldreich, P., & Reisenegger, A. 1992, ApJ, 395, 250
Gourgouliatos, K. N., & Cumming, A. 2015, MNRAS, 446, 1121
Graber, V., Cumming, A., & Andersson, N. 2018, ApJ, 865, 23
Harding, A. K., Stern, J. V., Dyks, J., & Frackowiak, M. 2008, ApJ, 680, 1378
Haskell, B. 2015, IJMPE, 24, 1541007
Haskell, B., Khomenko, V., Antonelli, M., & Antonopoulou, D. 2018, MNRAS, 481, L146
Haskell, B., Samuelsson, L., Glampedakis, K., & Andersson, N. 2008, MNRAS, 385, 531
Haskell, B., & Sedrakian, A. 2018, Ap&SS Libr., 457, 401
Ho, W. C. G., & Andersson, N. 2011, PhRvL, 107, 101101
Ho, W. C. G., & Andersson, N. 2012, NatPh, 8, 787
Ho, W. C. G., Espinoza, C. M., Antonopoulou, D., & Andersson, N. 2015, SciA, 1, e1500578
Horvath, J. E. 2019, MNRAS, 484, 1983
Jones, P. B. 1976, Ap&SS, 45, 369
Kojima, Y., & Suzuki, K. 2020, MNRAS, 494, 3790
Kou, F. F., & Tong, H. 2015, MNRAS, 450, 1990
Li, A., Dong, J. M., Wang, J. B., & Xu, R. X. 2016, ApJS, 223, 16
Li, X., Jiang, Z. J., & Zhang, L. 2013, ApJ, 765, 124
Link, B., Epstein, R. I., & Lattimer, J. M. 1999, PhRvL, 83, 3362
Livingstone, M. A., Kaspi, V. M., Gavriil, F. P., et al. 2007, Ap&SS, 308, 317
Lyne, A. G., Jordan, C. A., Graham-Smith, F., et al. 2015, MNRAS, 446, 857
Lyne, A. G., Pritchard, R. S., & Graham-Smith, F. 1993, MNRAS, 265, 1003
Lyne, A. G., Pritchard, R. S., Graham-Smith, F., & Camilo, F. 1996, Natur, 381, 497
Marshall, F. E., Guillemot, L., Harding, A. K., Martin, P., & Smith, D. A. 2016, ApJL, 827, L39
Mastrano, A., & Melatos, A. 2012, MNRAS, 421, 760
Menou, K., Perna, R., & Hernquist, L. 2001, ApJL, 554, L63
Muslimov, A., & Page, D. 1996, ApJ, 458, 347
Nikitina, E. B., & Malov, I. F. 2017, ARep, 61, 591
Ostriker, J. P., & Gunn, J. E. 1969, ApJ, 157, 1395
Philippov, A., Tchekhovskoy, A., & Li, J. G. 2014, MNRAS, 441, 1879
Pizzochero, P. M., Antonelli, M., Haskell, B., & Seveso, S. 2017, NatAs, 1, 0134
Pons, J. A., Link, B., Miralles, J. A., & Geppert, U. 2007, PhRvL, 98, 071101
Rookyard, S. C., Weltevrede, P., & Johnston, S. 2015a, MNRAS, 446, 3356
Rookyard, S. C., Weltevrede, P., & Johnston, S. 2015b, MNRAS, 446, 3367
Roy, J., Gupta, Y., & Lewandowski, W. 2012, MNRAS, 424, 2213
Shapiro, S. L., & Teukolsky, S. A. 1983, Black Holes, White Dwarfs, and Neutron Stars: The Physics of Compact Objects (New York: Wiley)
Spitkovsky, A. 2006, ApJL, 648, L51
Stella, L., Dall'Osso, S., Israel, G. L., & Vecchio, A. 2005, ApJL, 634, L165
Tian, J. 2018, NewA, 61, 100
Wang, Y., Ng, C. W., Takata, J., et al. 2014, MNRAS, 445, 604
Watters, K. P., Romani, R. W., Weltevrede, P., & Johnston, S. 2009, ApJ, 695, 1289
Watts, A. L., Andersson, N., Chakrabarty, D., et al. 2016, RvMP, 88, 021001
Weltevrede, P., Johnston, S., & Espinoza, C. M. 2011, MNRAS, 411, 1917
Xu, R. X., & Qiao, G. J. 2001, ApJL, 561, L85
Zhou, X., Tong, H., Zhu, C., & Wang, N. 2017, MNRAS, 472, 2403